

Meta-RangeSeg: LiDAR Sequence Semantic Segmentation Using Multiple Feature Aggregation

Song Wang, Jianke Zhu, *Senior Member, IEEE*, Ruixiang Zhang

Abstract—LiDAR sensor is essential to the perception system in autonomous vehicles and intelligent robots. To fulfill the real-time requirements in real-world applications, it is necessary to efficiently segment the LiDAR scans. Most of previous approaches directly project 3D point cloud onto the 2D spherical range image so that they can make use of the efficient 2D convolutional operations for image segmentation. Although having achieved the encouraging results, the neighborhood information is not well-preserved in the spherical projection. Moreover, the temporal information is not taken into consideration in the single scan segmentation task. To tackle these problems, we propose a novel approach to semantic segmentation for LiDAR sequences named Meta-RangeSeg, where a novel range residual image representation is introduced to capture the spatial-temporal information. Specifically, Meta-Kernel is employed to extract the meta features, which reduces the inconsistency between the 2D range image coordinates input and Cartesian coordinates output. An efficient U-Net backbone is used to obtain the multi-scale features. Furthermore, Feature Aggregation Module (FAM) aggregates the meta features and multi-scale features, which tends to strengthen the role of range channel. We have conducted extensive experiments for performance evaluation on SemanticKITTI, which is the de-facto dataset for LiDAR semantic segmentation. The promising results show that our proposed Meta-RangeSeg method is more efficient and effective than the existing approaches.

Index Terms—3D semantic segmentation, LiDAR perception, autonomous vehicle

I. INTRODUCTION

LiDAR can accurately measure the range by taking advantage of its active sensor, which plays an increasingly important role in the perception system of modern autonomous vehicles and robotics. Due to the characteristics of disorder and irregularity, it is challenging to perform scene understanding on LiDAR sequences.

LiDAR semantic segmentation aims to estimate the labels for each point, which is the key to understand the surroundings for the perception system. During past decade, extensive research efforts have been devoted to this task. Point-based methods [1]–[3] directly extract features from the raw output of LiDAR sensor. However, point convolution is usually computational intensive. To address this issue, projection-based methods [4]–[6] and voxel-based approaches [7]–[9] convert the irregular raw point cloud data into regular grid representations so that the conventional convolutional layer

Song Wang and Jianke Zhu are with the College of Computer Science, Zhejiang University, Hangzhou, China, 310027. Ruixiang Zhang is with Hikvision Research Institute, Hangzhou, China, 310051.
E-mail: {songw,jkzhu}@zju.edu.cn, zxrisgood@gmail.com.

Jianke Zhu is the Corresponding Author.

Manuscript received April 19, 2021; revised August 16, 2021.

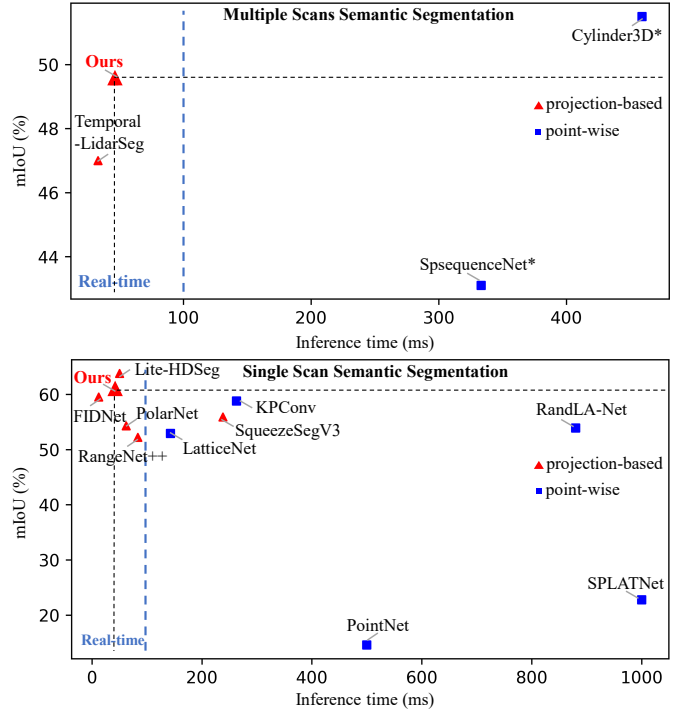


Fig. 1. Accuracy vs. inference time. * denotes the results reproduced from the original implementation. Our presented Meta-RangeSeg method obtains the promising results on both multiple scans and single scan semantic segmentation in SemanticKITTI benchmark [13] and runs at real-time.

for image can be employed. Nevertheless, they fail to preserve the original neighborhood relationship. In practice, the hybrid methods [10]–[12] fuse two or more of the above feature representations, which can obtain the better results. Unfortunately, this incurs the extra computational load.

Generally, scene analysis for autonomous driving is conducted within a sequence of LiDAR scans. Most of previous approaches only take into account of single frame in LiDAR semantic segmentation, where the important temporal information is usually ignored. Moreover, some methods [14], [15] aim to deal with multiple scans simultaneously. This may lead to information redundancy and slow inference speed, as shown in Fig. 1.

To tackle the above challenging problems, we propose a novel approach to semantic segmentation for LiDAR sequences named Meta-RangeSeg, where a novel range residual image representation is introduced to capture the spatial-temporal information. In contrast to the direct fusion method, our proposed range residual image efficiently represents multi-frame point cloud information, which can improve the accu-

racy and the speed of training and testing under the limited computing resources. Since the range residual image obtained from spherical projection may not effectively capture the local geometric structures, we take advantage of the Meta-Kernel operator [16] to extract the meta features by dynamically learning the weights from the relative Cartesian coordinates and range values. Thus, it reduces the inconsistency between the 2D range image coordinates input and Cartesian coordinates output. Moreover, an efficient U-Net backbone is used to obtain the multi-scale features. Furthermore, Feature Aggregation Module (FAM) aggregates the meta features and multi-scale features, which tends to strengthen the role of the range channel. We have conducted extensive experiments for performance evaluation on SemanticKITTI, which is the de-facto dataset for LiDAR semantic segmentation. The promising results show that our proposed Meta-RangeSeg method is more efficient and effective than the existing approaches.

In summary, the main contributions of this paper are: 1) a novel approach to semantic segmentation on LiDAR sequences by taking advantage of range residual image, which is able to efficiently capture the spatial-temporal information; 2) an effective Meta-Kernel feature extraction method for LiDAR semantic segmentation; 3) a Feature Aggregation Module (FAM) to aggregate meta features at various scales for object segmentation; 4) experiments on SemanticKITTI benchmark show that our proposed approach is promising.

II. RELATED WORK

With the prevalence of autonomous driving, a surge of research efforts have been spent on semantic scene understanding. In this work, we focus on the task of semantic segmentation using LiDAR scans [13], [17]. Generally, most of existing studies on LiDAR semantic segmentation can be categorized into four groups according to the different feature representations, including point, range map, voxel and hybrid.

Point-based methods directly extract features from the raw output of LiDAR sensor, which are able to preserve the 3D spatial structure information. Due to irregularity of point cloud data, it is challenging to design the efficient neural network layer for it. Qi *et al.* [1] extract the deep features on point cloud by the shared Multi-Layer Perceptrons (MLP) for classification and segmentation. The subsequent series of works [2], [18] try to address the limitation in extracting local features, which obtain the encouraging results on the indoor semantic segmentation. The main showstopper for these approaches is their high computational cost and memory consumption, which hinders them from the large-scale outdoor driving scenarios. One remedy is to reduce their time complexity and information loss by randomly sampling and local feature aggregation [3]. Despite of its efficiency on the large scenes, there is noticeable performance drop due to sub-sampling.

Voxel representation is able to make use of the 3D convolution neural network that can effectively solve the irregularity problem. The regular 3D dense convolutions for semantic segmentation [19], [20] requires the huge memory and heavy computational power for the fine resolution, which limit their capability of processing the large scale outdoor LiDAR scans.

To this end, the sparse convolution [7], [9] is employed to reduce the computational cost. Zhu *et al.* [15] propose a voxel division method with asymmetric convolution based on LiDAR point cloud distribution.

By projecting 3D point cloud onto 2D space, range map is a promising representation, which can take advantage of a large amount of advanced layers for image feature extraction with fast inference and training. To account for the mechanism of LiDAR scanning, most of existing LiDAR semantic segmentation approaches [5], [6], [21], [22] make use of spherical projection to obtain range images. Besides range view (RV), Zhang *et al.* [23] employ a bird's-eye view (BEV) for semantic segmentation. Some studies [24], [25] consider to combine these two different projection methods in order to achieve more accurate segmentation results. However, this will lead to the extra memory consumption and computational overhead. Moreover, directly fusing two different projections ignores the underlying geometric structure of LiDAR scan.

The hybrid approach intends to fuse the different feature representations for better LiDAR semantic segmentation. Zhang *et al.* [10] propose a point-voxel interaction MLP network that aggregates features among neighborhood voxels and their corresponding points. Thereby, it is able to avoid the time-consuming neighborhood search while achieving the encouraging results on outdoor LiDAR data. Tang *et al.* [11] present an efficient point-voxel fusion pipeline. Voxels provide the coarse-grained local features, and points preserve the fine-grained geometric features through a simple MLP. Xu *et al.* [12] fuse three different feature representations, including point, range map and voxel, which achieve the promising fusion results by interacting features at various stages.

Most of existing approaches perform the LiDAR semantic segmentation on single scan, where the temporal information is usually neglected. There are only few methods focusing on the multiple scans task. Shi *et al.* [14] employ a voxel-based 3D sparse convolutional network to fuse local information from the previous and current frames through local interpolation, which only make use of the two consecutive scans. Duerr *et al.* [26] propose a recurrent segmentation architecture using range images, which recursively aggregate the features of previous scans in order to exploit the short term temporal dependencies. In [15], superimposing point clouds in 3D space is adopted for multiple scans segmentation, whose memory consumption and computational time increase linearly with the total number of scans per input model. In this paper, we introduce an efficient range residual image representation, where the effective features can be extracted by Meta-Kernel.

III. META-RANGESEG FOR LiDAR SEMANTIC SEGMENTATION

In this section, we present an efficient neural network Meta-RangeSeg for LiDAR semantic segmentation on multiple scans.

A. Overview

In this paper, we aim to predicting the semantic labels from the consecutive LiDAR sequences. Unlike the conventional

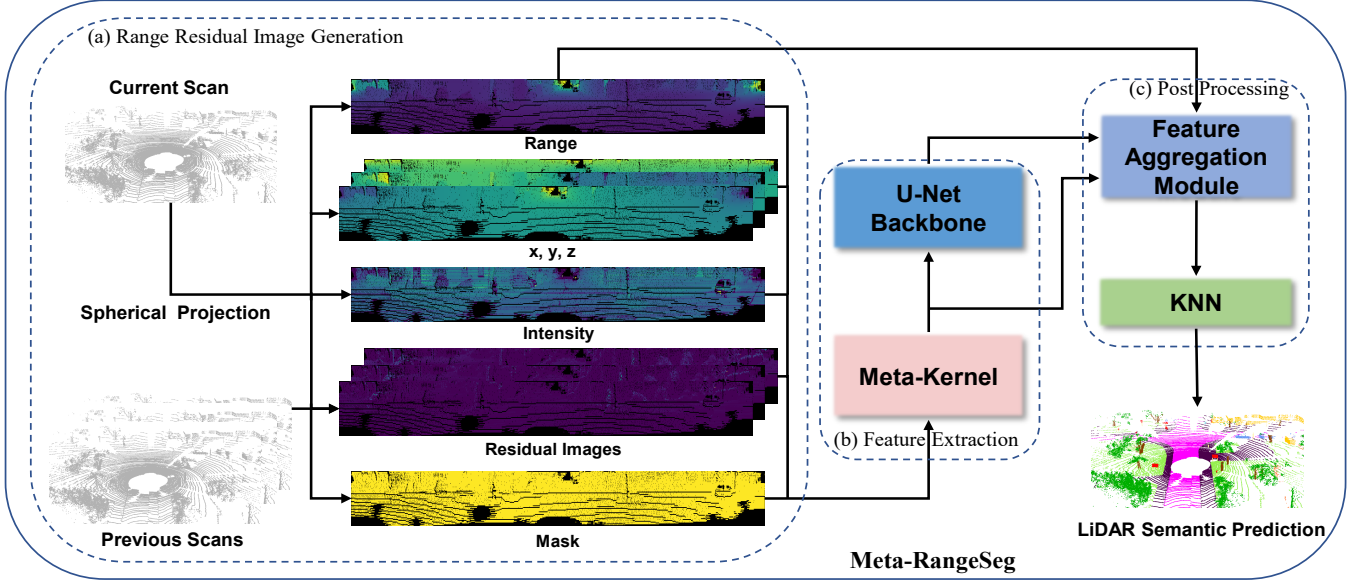


Fig. 2. Our proposed Meta-RangeSeg framework. (a) Calculate range residual image with nine channels capturing spatial and motion information of raw data. (b) Extract meta features by Meta-Kernel and obtain multi-scale features via U-Net Backbone. (c) Aggregate features and get semantic labels in 3D space.

approaches transforming the sequential point cloud into global coordinates [14], [15], we suggest a novel Meta-RangeSeg approach to efficiently process multiple scans in range view for the subsequent feature extraction.

As shown in Fig. 2, our proposed network takes advantage of the range residual image with nine channels built from the current scan and previous ones. Then, the meta feature is extracted by a Meta-Kernel block, and the multi-scale feature is obtained via a U-Net network. Finally, we obtain the final labels for raw data by post-processing the aggregated features. To facilitate the effective semantic segmentation, we train the proposed neural network by the loss function \mathcal{L} with three different terms as follows:

$$\mathcal{L} = w_1 \mathcal{L}_{wce} + w_2 \mathcal{L}_{ls} + w_3 \mathcal{L}_{bd}, \quad (1)$$

where \mathcal{L}_{wce} is the weighted cross-entropy loss, and \mathcal{L}_{ls} is the Lovász loss. \mathcal{L}_{bd} is the Boundary loss. w_1 , w_2 and w_3 are the weights with respect to each term. In our implementation, we set $w_1 = 1$, $w_2 = 1.5$ and $w_3 = 1$, empirically.

To account for the multi-class segmentation problem, the weighted cross-entropy loss \mathcal{L}_{wce} [27] is employed to maximize the prediction accuracy for point labels, which is able to balance the distributions among different classes by weighting the cross-entropy loss with the inverse square root of class frequency f_i as

$$\mathcal{L}_{wce}(y, \hat{y}) = - \sum_i \frac{1}{\sqrt{f_i}} p(y_i) \log(p(\hat{y}_i)), \quad (2)$$

where y_i represents the ground truth, and \hat{y}_i is prediction.

The Lovász loss \mathcal{L}_{ls} [28] is used to maximize the intersection-over-union (IoU) score that is commonly used to in performance evaluation on semantic segmentation. Since IoU is discrete and indifferentiable, it needs to be optimized using a derivable surrogate function. We define a vector of pixel errors $\mathbf{m}(c)$ of each pixel i on class c with its

predicted probability $f_i(c) \in [0, 1]$ and ground truth label $y_i(c) \in \{-1, 1\}$:

$$m_i(c) = \begin{cases} 1 - f_i(c) & \text{if } c = y_i(c), \\ f_i(c) & \text{otherwise} \end{cases} \quad (3)$$

We use the Lovász extension [28] for the vector of errors $\mathbf{m}(c)$ to construct the loss $\overline{\Delta}_{J_c}$ surrogate to Δ_{J_c} . Then, \mathcal{L}_{ls} can be formulated as below:

$$\mathcal{L}_{ls} = \frac{1}{|C|} \sum_{c \in C} \overline{\Delta}_{J_c}(\mathbf{m}(c)), \quad (4)$$

where $|C|$ denotes the total number of classes.

As suggested in [29], the pixel-level loss function like cross-entropy may not effectively handle the complex boundaries between different classes in remote sensing images that have wide range and low contrast. To emphasize the boundaries between different objects, we adopt the boundary loss function \mathcal{L}_{bd} [29] for LiDAR semantic segmentation. Given the extracted boundary map y^b for ground truth y and \hat{y}^b for the predicted result \hat{y} in the range view, \mathcal{L}_{bd} is defined as below:

$$\mathcal{L}_{bd}(y, \hat{y}) = 1 - \frac{2P_b^c R_b^c}{P_b^c + R_b^c}, \quad (5)$$

where P_b^c and R_b^c define the precision and recall of boundary map \hat{y}^b to y^b for class c . The boundary map is calculated as follows:

$$\begin{aligned} y^b &= \text{pool}(1 - y, \theta_0) - (1 - y) \\ \hat{y}^b &= \text{pool}(1 - \hat{y}, \theta_0) - (1 - \hat{y}) \end{aligned} \quad (6)$$

where $\text{pool}(\cdot, \cdot)$ is a pixel-wise max-pooling operation on the inverted ground truth binary map or predictions with a sliding window of size $\theta_0 = 3$.

B. Range Residual Image

Range image representation has the advantage of the effective 2D operations for fast training and inference. To this end, we map the scattered LiDAR points onto their corresponding 2D spherical coordinates through a mapping function $\mathbb{R}^3 \rightarrow \mathbb{R}^2$ as below:

$$\begin{pmatrix} u \\ v \end{pmatrix} = \begin{pmatrix} \frac{1}{2} [1 - \arctan(y, x) \pi^{-1}] & W \\ [1 - (\arcsin(z r^{-1}) + f_{\text{up}}) f^{-1}] & H \end{pmatrix}, \quad (7)$$

where (u, v) are image coordinates, and (H, W) are the height and width of the desired range image representation. $f = f_{\text{up}} + f_{\text{down}}$ is the vertical field-of-view of the sensor, and $r = \sqrt{x^2 + y^2 + z^2}$ is the range of each point.

Motivated by the residual image feature for segmenting moving objects in video analysis [30], [31], we introduce it into the task of semantic segmentation on LiDAR sequences to capture the temporal information. Based on the range images from current scan and previous frames using spherical projection, the input of our proposed neural network is made of range images and their residuals, as illustrated in Fig. 2. Specifically, it is a range residual image with the size of $9 \times H \times W$, where each pixel (u_i, v_i) contains a vector $(r_i, x_i, y_i, z_i, e_i, d_{1,i}^0, d_{2,i}^0, d_{3,i}^0, m_i)$. m_i indicates whether the pixel position is a projected point or not. d_j^0 is the residual image that calculates the range difference between the previous j^{th} scan and the current one. We use the last three LiDAR scans in our implementation.

To effectively fuse different scans, residual image is calculated in the following three steps. We firstly compensate the ego-motion by transforming the previous scans into the current local coordinates. Secondly, the transformed scans are re-projected into the current range image view using Eq. (7). Finally, we compute the residual $d_{k,i}^l$ for each pixel i by calculating the normalized absolute differences between the ranges of current scan and the transformed one by

$$d_{k,i}^l = \frac{|r_i - r_i^{k \rightarrow l}|}{r_i}, \quad (8)$$

where r_i is the range value in current scan located at range image coordinates (u_i, v_i) , and $r_i^{k \rightarrow l}$ is the corresponding range value from the transformed scan located at the same image position.

C. Feature Extraction

To facilitate the effective LiDAR semantic segmentation, we design a feature extraction module that consists of a Meta-Kernel block and a U-Net backbone, as shown in Fig. 2.

In our empirical study, the conventional convolution operations do not perform well on the range residual image. To address this issue, we take advantage of the Meta-Kernel block to extract the meta features by dynamically learning the weights from the relative Cartesian coordinates and range values. As in [16], the Meta-Kernel is designed to effectively locate objects in LiDAR scans by exploiting the geometric information from the Cartesian coordinates. In this paper, we employ it to capture the spatial and temporal information for semantic segmentation.

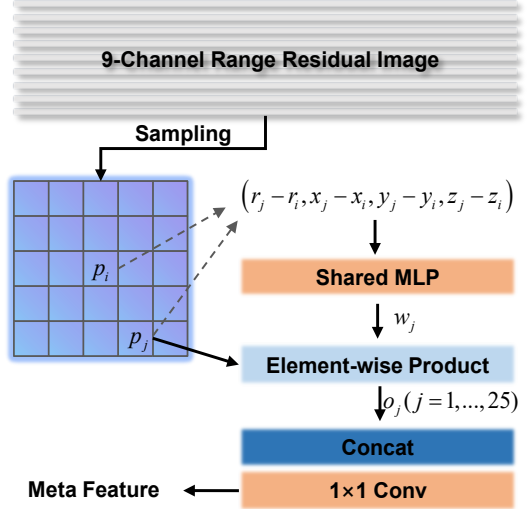


Fig. 3. Illustration of Meta-Kernel. We sample the range residual image using a 5×5 sliding window and learn weights dynamically from the relative Cartesian coordinates and range value to extract meta features.

In order to achieve a larger receptive field on the range residual image for Meta-Kernel, we enlarge the size of sliding window into 5×5 . Therefore, we can get the relative Cartesian coordinates of 25 neighbors $\mathbf{p}_j(x_j, y_j, z_j)$ for the center $\mathbf{p}_i(x_i, y_i, z_i)$: $(x_j - x_i, y_j - y_i, z_j - z_i)$. More importantly, the range difference is added to enhance the perception of spatial information. Furthermore, a shared MLP employed to generate 25 weight vectors from the input $(r_j - r_i, x_j - x_i, y_j - y_i, z_j - z_i)$. We multiply the learned weight vectors \mathbf{w}_j element-wisely with the channel information $(r_j, x_j, y_j, z_j, e_j, d_{1,j}^0, d_{2,j}^0, d_{3,j}^0, m_j)$ at its corresponding position within the sliding window. Finally, a 1×1 convolution is used to obtain the meta features, which aggregates the information from different channels and different sampling locations. From the above all, the whole process of Meta-Kernel block is summarized into Fig. 3.

We obtain the multi-scale features through the U-Net backbone that is an encoder-decoder architecture commonly used in semantic segmentation [6], [32]. Specifically, we firstly employ four down-sampling layers to extract the features of different scales from meta features, and then restore the original resolution through four up-sampling layers. Moreover, skip connection is adopted to assist in reconstructing high-resolution information.

D. Post Processing

Once the meta and multi-scale features are obtained, we perform feature aggregation to predict the labels from range perspective. To this end, the Feature Aggregation Module is designed to make use of range information for object segmentation in the different ranges by aggregating features at various scales, as shown in Fig. 4.

The range channel is extracted separately, which is further fed into the context module [6] to capture the global context with the more detailed range information. Then, we fuse the range features with multi-scale features through an attention

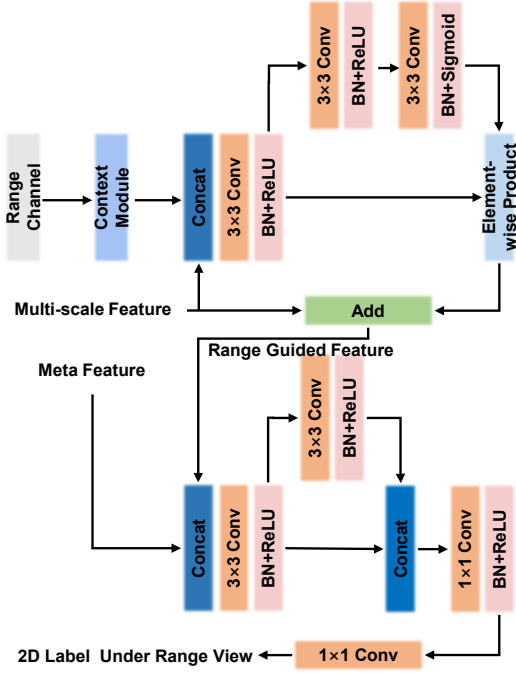


Fig. 4. Illustration of Feature Aggregation Module (FAM). We firstly extract the features of the range channel separately, and then fuse the multi-scale and the range features to obtain the range-guided features. Finally, the meta and range-guided features are aggregated via skip connection, and the 2D label under range view is obtained through 1×1 convolution layer.

fusion layer. To this extent, the range-guided features are able to fuse the range context information and semantic features. Inspired by ResNet [33], the meta features are reused through skip connections. We concatenate the meta features with the range-guided features. Afterwards, the final features are fused through the convolution and residual connection. Thus, we can obtain the 2D labels under the range view via a 1×1 convolution layer.

To estimate the full labels in 3D space from 2D predictions in range view, we employ k -Nearest Neighborhood in the post-processing stage. During the spherical projection, there may be multiple points projected into the same grid. We sort the points according to their ranges, and the characteristics of the closer points within the range shall prevail. When recovering 3D information from 2D range residual image, we need to supplement the features of those missing points. In k -NN, the label of each point is jointly determined by its k closest points. Instead of using Euclidean distance, range information is employed as the similarity measure so that we can efficiently process data using the sliding windows in 2D space. As described in [5], the k -nearest points within a window can represent the distribution in 3D space very well. In our implementation, we set $k = 5$ with a 7×7 sliding window.

E. Training

We trained the proposed neural network for 180 epochs using the stochastic gradient descent (SGD) on a PC with two RTX 2080Ti GPUs. The total batch size is 4. Moreover, the initial learning rate is set to 0.01, which is decayed by 0.0001

after each epoch. We conducted the inference on a single RTX 2080Ti GPU. The height and width of the range residual image are set to $H = 64$, and $W = 2048$, respectively. During the training process, we perform data augmentation by randomly rotating, transforming, and flipping the 3D point cloud. In addition, we randomly drop the points at a percentage with a uniform distribution between 0 and 10 before creating the range residual image.

IV. EXPERIMENT

In this section, we give the details of our experiments and show the results on LiDAR semantic segmentation. Moreover, we compare our proposed approach against the state-of-the-art method and discuss the results on different settings.

A. Dataset

The SemanticKITTI dataset [13] is a large-scale outdoor scene LiDAR dataset, which provides the dense point-wise annotations for all 22 sequences in KITTI Odometry Benchmark [34]. Sequence 00 to 10 are treated as the training sets, and Sequence 11 to 21 are used as test sets. There are 23,201 and 20,351 complete 3D scans for training and testing, respectively. We follow the setting in [13], and keep Sequence 08 as the validation set. To evaluate the effectiveness of our proposed approach, we submit the output to the online evaluation website to obtain the results on the testing set.

B. Evaluation Metric

To facilitate the fair comparison, we evaluate the performance of different methods with respect to the mean intersection over union metric (mIoU) [13], which is defined as below:

$$mIoU = \frac{1}{n} \sum_{c=1}^n \frac{TP_c}{TP_c + FP_c + FN_c}. \quad (9)$$

For class c , TP_c represents the true positives, and FP_c denotes false positives. FN_c is false negative predictions. In SemanticKITTI benchmark, the single scan task evaluates 19 different classes ($n = 19$). On the other hand, the multiple scans task evaluates 25 different classes ($n = 25$), which needs to distinguish more than 6 moving classes comparing to the single-scan challenge.

C. Performance Evaluation

For the quantitative evaluation, we compare our proposed approach against other methods on the multiple scans task in semantic segmentation benchmark. As shown in Table I, our presented Meta-RangeSeg method outperforms the state-of-the-art approach [26] by 2.5% on SemanticKITTI test set, which also achieves the best results on the most of classes. It is worthy of mentioning that our approach can process the input point cloud data at a rate of 22Hz while maintaining high accuracy. It is faster than the frame rate of sensor, i.e., 10 Hz for a typical spinning 3D LiDAR sensor.

Considering that there are few methods in the multiple scans semantic segmentation evaluation, we also conduct experiments on the single scan task. For a fair comparison, we only

TABLE I

COMPARISONS ON THE OFFICIAL SEMANTICKITTI MULTIPLE SCANS BENCHMARK. THE ITEM WITH ARROW INDICATES THE MOVING CLASS. VALUES ARE GIVEN AS IOU (%).

Methods	mean-IoU	car	bicycle	motorcycle	truck	other-vehicle	person	bicyclist	motorcyclist	road	parking	sidewalk	other-ground	building	fence	vegetation	trunk	terrain	pole	traffic sign	car	bicyclist	motorcyclist	person	other-vehicle	truck
	car	bicycle	motorcycle	truck	other-vehicle	person	bicyclist	motorcyclist	road	parking	sidewalk	other-ground	building	fence	vegetation	trunk	terrain	pole	traffic sign	car	bicyclist	motorcyclist	person	other-vehicle	truck	
TangentConv [35]	34.1	84.9	2.0	18.2	21.1	18.5	1.6	0.0	0.0	83.9	38.3	64.0	15.3	85.8	49.1	79.5	43.2	56.7	36.4	31.2	40.3	1.1	6.4	1.9	30.1	42.2
DarkNet53Seg [13]	41.6	84.1	30.4	32.9	20.2	20.7	7.5	0.0	0.0	91.6	64.9	75.3	27.5	85.2	56.5	78.4	50.7	64.8	38.1	53.3	61.5	14.1	15.2	0.2	28.9	37.8
SpSequenceNet [14]	43.1	88.5	24.0	26.2	29.2	22.7	6.3	0.0	0.0	90.1	57.6	73.9	27.1	91.2	66.8	84.0	66.0	65.7	50.8	48.7	53.2	41.2	26.2	36.2	2.3	0.1
TemporalLidarSeg [26]	47.0	92.1	47.7	40.9	39.2	35.0	14.4	0.0	0.0	91.8	59.6	75.8	23.2	89.8	63.8	82.3	62.5	64.7	52.6	60.4	68.2	42.8	40.4	12.9	12.4	2.1
Meta-RangeSeg(Ours)	49.5	90.1	52.7	43.9	30.3	35.4	14.3	0.0	0.0	90.7	63.3	74.7	26.9	90.5	63.5	83.0	67.0	67.7	56.4	64.4	64.5	56.1	55.0	24.4	20.3	3.4

TABLE II

COMPARISONS ON THE OFFICIAL SEMANTICKITTI SINGLE SCAN BENCHMARK. \ddagger DENOTES THE SECOND BEST RESULTS. THE UPPER-HALF SHOWS THE POINT-WISE METHODS, AND THE LOWER-HALF ARE PROJECTION-BASED METHODS.

Methods	Size	mean-IoU	car	bicycle	motorcycle	truck	other-vehicle	person	bicyclist	motorcyclist	road	parking	sidewalk	other-ground	building	fence	vegetation	trunk	terrain	pole	traffic-sign
		car	bicycle	motorcycle	truck	other-vehicle	person	bicyclist	motorcyclist	road	parking	sidewalk	other-ground	building	fence	vegetation	trunk	terrain	pole	traffic-sign	
PointNet [1]	50K pts	14.6	46.3	1.3	0.3	0.1	0.8	0.2	0.2	0.0	61.6	15.8	35.7	1.4	41.4	12.9	31.0	4.6	17.6	2.4	3.7
PointNet++ [2]	50K pts	20.1	53.7	1.9	0.2	0.9	0.2	0.9	1.0	0.0	72.0	18.7	41.8	5.6	62.3	16.9	46.5	13.8	30.0	6.0	8.9
SPLATNet [36]	50K pts	22.8	66.6	0.0	0.0	0.0	0.0	0.0	0.0	0.0	70.4	0.8	41.5	0.0	68.7	27.8	72.3	35.9	35.8	13.8	0.0
TangentConv [35]	50K pts	35.9	86.8	1.3	12.7	11.6	10.2	17.1	20.2	0.5	82.9	15.2	61.7	9.0	82.8	44.2	75.5	42.5	55.5	30.2	22.2
LatticeNet [37]	50K pts	52.9	92.9	16.6	22.2	26.6	21.4	35.6	43.0	46.0	90.0	59.4	74.1	22.0	88.2	58.8	81.7	63.6	63.1	51.9	48.4
RandLa-Net [3]	50K pts	53.9	94.2	26.0	25.8	40.1	38.9	49.2	48.2	7.2	90.7	60.3	73.7	20.4	86.9	56.3	81.4	61.3	66.8	49.2	47.7
KPConv [18]	50K pts	58.8	96.0	30.2	42.5	33.4	44.3	61.5	61.6	11.8	88.8	61.3	72.7	31.6	90.5	64.2	84.8	69.2	69.1	56.4	47.4
BAAF-Net [38]	50K pts	59.9	95.4	31.8	35.5	48.7	46.7	49.5	55.7	33.0	90.9	62.2	74.4	23.6	89.8	60.8	82.7	63.4	67.9	53.7	52.0
RangeNet53++ [5]	64 \times 2048	52.2	91.4	25.7	34.4	25.7	23.0	38.3	38.8	4.8	91.8	65.0	75.2	27.8	87.4	58.6	80.5	55.1	64.6	47.9	55.9
PolarNet [23]	[480, 360, 32]	54.3	93.8	40.3	30.1	22.9	28.5	43.2	40.2	5.6	90.8	61.7	74.4	21.7	90.0	61.3	84.0	65.5	67.8	51.8	57.5
MINet [39]	64 \times 2048	55.2	90.1	41.8	34.0	29.9	23.6	51.4	52.4	25.0	90.5	59.0	72.6	25.8	85.6	52.3	81.1	58.1	66.1	49.0	59.9
3D-MiniNet [22]	64 \times 2048	55.8	90.5	42.3	42.1	28.5	29.4	47.8	44.1	14.5	91.6	64.2	74.5	25.4	89.4	60.8	82.8	60.8	66.7	48.0	56.6
SqueezeSegV3 [21]	64 \times 2048	55.9	92.5	38.7	36.5	29.6	33.0	45.6	46.2	20.1	91.7	63.4	74.8	26.4	89.0	59.4	82.0	58.7	65.4	49.6	58.9
SalsaNext [6]	64 \times 2048	59.5	91.9	48.3	38.6	38.9	31.9	60.2	59.0	19.4	91.7	63.7	75.8	29.1	90.2	64.2	81.8	63.6	66.5	54.3	62.1
FIDNet [40]	64 \times 2048	59.5	93.9	54.7	48.9	27.6	23.9	62.3	59.8	23.7	90.6	59.1	75.8	26.7	88.9	60.5	84.5	64.4	69.0	53.3	62.8
Lite-HDSeg [41]	64 \times 2048	63.8	92.3	40.0	55.4	37.7	39.6	59.2	71.6	54.1	93.0	68.2	78.3	29.3	91.5	65.0	78.2	65.8	65.1	59.5	67.7
Meta-RangeSeg(Ours)	64 \times 2048	61.0 \ddagger	93.9	50.1	43.8	43.9	43.2	63.7	53.1	18.7	90.6	64.3	74.6	29.2	91.1	64.7	82.6	65.5	65.5	56.3	64.2

use the range image by excluding the residual image when extracting features under range view for the single scan evaluation. As shown in Table II, Meta-RangeSeg outperforms most of previous methods under the same settings, including point-wise and projection-based methods, which demonstrates the effectiveness of our proposed approach on LiDAR semantic segmentation.

For the qualitative evaluation, Fig. 5 shows some sample semantic segmentation results on the SemanticKITTI validation set. The range view is generated by Meta-RangeSeg method with the complete semantic labels. To investigate the performance of our approach on multiple scans semantic segmentation, we take car classes including static and moving as examples to compare the predicted visual results with the ground truth and predictions generated by SpsequenceNet [14], as illustrated in Fig. 6. It can be observed that our approach can effectively distinguish both static and moving objects with their semantic information.

D. Ablation Study

To examine the improvements of each individual module in our proposed network, we conduct the ablation studies on Sub-SemanticKITTI dataset, which is a subset of the original SemanticKITTI benchmark. Specifically, the training set of Sub-

SemanticKITTI dataset consists of every 8th frame in sequence 00-10 (except 08). The validation set is formed by every 4th frame in sequence 08. As only 1/8 training data and 1/4 validation data are used, we can quickly perform the evaluation.

For fair comparison, we treat Salsanext [6] with a 5-channel range image as the baseline method, which uses the similar backbone network as ours. In our experiments, we report the results on multiple scans semantic segmentation task. As shown in Table III, our proposed range residual image (R^2 Image) with 9 channels outperforms the baseline around 0.5%, which demonstrates that the range residual is effective. Moreover, the Meta-kernel block obtains over 0.9% improvement comparing the the method without it. Furthermore, FAM performs better than the network without it around 0.9%. Additionally, the boundary loss achieves over 1.8% performance gain, which indicates that the boundary regions are essential to the LiDAR semantic segmentation. Finally, it can be observed that our proposed Meta-RangeSeg approach outperforms the baseline over 4.1%, which demonstrates the efficacy of each module. Although having added the extra blocks into the backbone, the inference speed of the final model is not greatly affected. This is mainly due to the concise input and mature convolution operations.

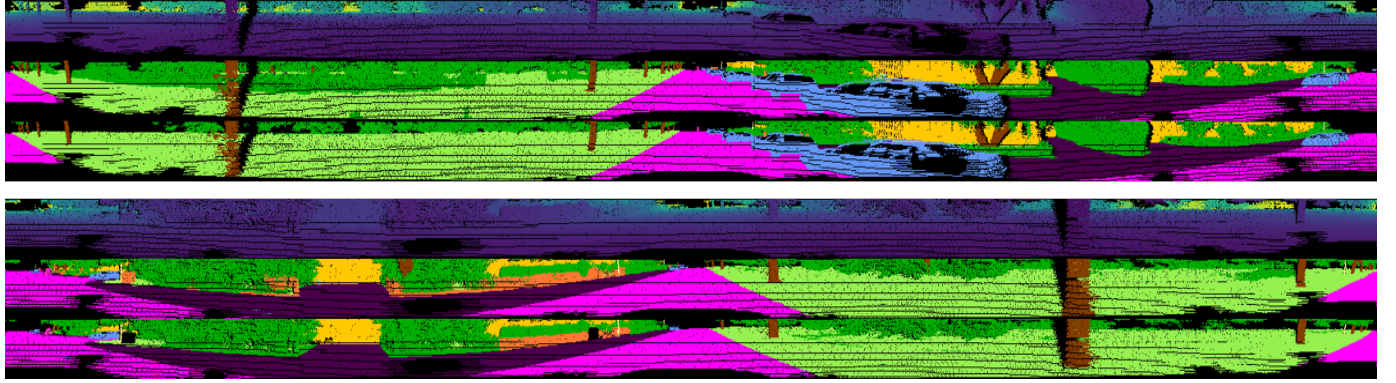


Fig. 5. Semantic segmentation results from the range view on the SemanticKITTI validation set (sequence 08) [best view in color]. In each scene, we show the range channel image, predictions by Meta-RangeSeg, and ground truth in turn.

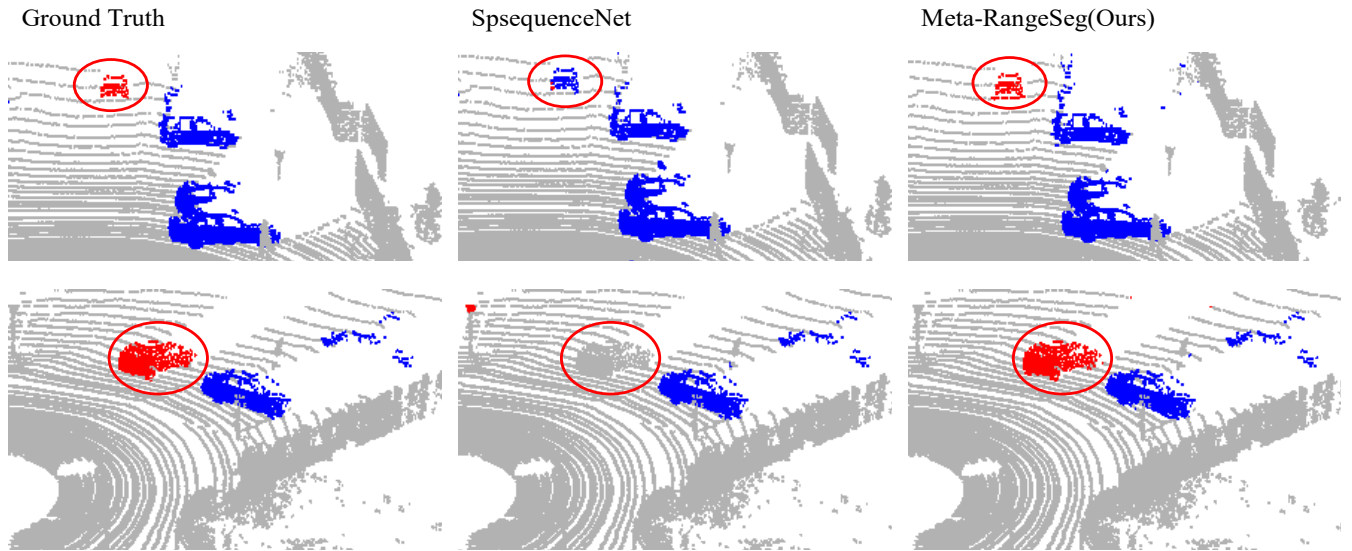


Fig. 6. Segmentation results of static and moving cars on the SemanticKITTI validation set (sequence 08). The static cars are labeled in blue, and moving cars are in red [best view in color]. At each row, the left is the ground truth, the middle is the predictions by SpsequenceNet [14], and the right is the results of our proposed Meta-RangeSeg approach.

TABLE III

ABLATIVE ANALYSIS EVALUATED ON VALIDATION SET (SEQ 08) IN SUB-SEMANICKITTI DATASET.

Architecture	R ² Image	Meta-Kernel	FAM	Boundary Loss	mIoU
Baseline	\times	\times	\times	\times	42.8
Meta-RangeSeg	✓	\times	\times	\times	43.3
	✓	✓	\times	\times	44.2
	✓	✓	✓	\times	45.1
	✓	✓	✓	✓	46.9

V. CONCLUSION

This paper proposed a novel approach to LiDAR semantic segmentation, which introduced a range residual image representation to capture the spatial-temporal information. Moreover, we employed Meta-Kernel to extract the meta features from the residual image by dynamically learning the weights from the relative Cartesian coordinates and range values. Furthermore, we designed a Feature Aggregation Mod-

ule to aggregate the meta features at various scales while emphasizing the range channel. We have conducted extensive evaluations on SemanticKITTI benchmark, whose promising results demonstrated that our proposed Meta-RangeSeg approach not only outperforms the state-of-the-art multiple scans semantic segmentation methods but also runs at 22 FPS.

Since some modules are not fully optimized, our model consumes more memory. In future, we will try to design an effective model that can make use of the connections between each channel in range residual image.

REFERENCES

- [1] C. R. Qi, H. Su, K. Mo, and L. J. Guibas, “Pointnet: Deep learning on point sets for 3d classification and segmentation,” in *Proceedings of the IEEE Conference on Computer Vision and Pattern Recognition (CVPR)*, 2017, pp. 652–660.
- [2] C. R. Qi, L. Yi, H. Su, and L. J. Guibas, “Pointnet++: Deep hierarchical feature learning on point sets in a metric space,” *Proceedings of the Advances in Neural Information Processing Systems (NIPS)*, vol. 30, 2017.
- [3] Q. Hu, B. Yang, L. Xie, S. Rosa, Y. Guo, Z. Wang, N. Trigoni, and A. Markham, “Randla-net: Efficient semantic segmentation of large-scale point clouds,” in *Proceedings of the IEEE/CVF Conference on*

Computer Vision and Pattern Recognition (CVPR), 2020, pp. 11 108–11 117.

[4] B. Wu, A. Wan, X. Yue, and K. Keutzer, “Squeezeseg: Convolutional neural nets with recurrent crf for real-time road-object segmentation from 3d lidar point cloud,” in *Proceedings of the IEEE International Conference on Robotics and Automation (ICRA)*. IEEE, 2018, pp. 1887–1893.

[5] A. Milioto, I. Vizzo, J. Behley, and C. Stachniss, “Rangenet++: Fast and accurate lidar semantic segmentation,” in *Proceedings of the IEEE/RSJ International Conference on Intelligent Robots and Systems (IROS)*. IEEE, 2019, pp. 4213–4220.

[6] T. Cortinhal, G. Tzlepis, and E. E. Aksoy, “Salsanext: Fast, uncertainty-aware semantic segmentation of lidar point clouds for autonomous driving,” *arXiv preprint arXiv:2003.03653*, 2020.

[7] B. Graham, M. Engelcke, and L. Van Der Maaten, “3d semantic segmentation with submanifold sparse convolutional networks,” in *Proceedings of the IEEE Conference on Computer Vision and Pattern Recognition (CVPR)*, 2018, pp. 9224–9232.

[8] L. Han, T. Zheng, L. Xu, and L. Fang, “Occuseg: Occupancy-aware 3d instance segmentation,” in *Proceedings of the IEEE/CVF Conference on Computer Vision and Pattern Recognition (CVPR)*, 2020, pp. 2940–2949.

[9] R. Cheng, R. Razani, E. Taghavi, E. Li, and B. Liu, “2-s3net: Attentive feature fusion with adaptive feature selection for sparse semantic segmentation network,” in *Proceedings of the IEEE/CVF Conference on Computer Vision and Pattern Recognition (CVPR)*, 2021, pp. 12 547–12 556.

[10] F. Zhang, J. Fang, B. Wah, and P. Torr, “Deep fusionnet for point cloud semantic segmentation,” in *Proceedings of the European Conference on Computer Vision (ECCV)*, vol. 2, 2020, p. 6.

[11] H. Tang, Z. Liu, S. Zhao, Y. Lin, J. Lin, H. Wang, and S. Han, “Searching efficient 3d architectures with sparse point-voxel convolution,” in *Proceedings of the European Conference on Computer Vision (ECCV)*. Springer, 2020, pp. 685–702.

[12] J. Xu, R. Zhang, J. Dou, Y. Zhu, J. Sun, and S. Pu, “Rpnet: A deep and efficient range-point-voxel fusion network for lidar point cloud segmentation,” in *Proceedings of the IEEE/CVF International Conference on Computer Vision (ICCV)*, 2021, pp. 16 024–16 033.

[13] J. Behley, M. Garbade, A. Milioto, J. Quenzel, S. Behnke, C. Stachniss, and J. Gall, “Semantickitti: A dataset for semantic scene understanding of lidar sequences,” in *Proceedings of the IEEE/CVF International Conference on Computer Vision (ICCV)*, 2019, pp. 9297–9307.

[14] H. Shi, G. Lin, H. Wang, T.-Y. Hung, and Z. Wang, “Spsequencenet: Semantic segmentation network on 4d point clouds,” in *Proceedings of the IEEE/CVF Conference on Computer Vision and Pattern Recognition (CVPR)*, 2020, pp. 4574–4583.

[15] X. Zhu, H. Zhou, T. Wang, F. Hong, W. Li, Y. Ma, H. Li, R. Yang, and D. Lin, “Cylindrical and asymmetrical 3d convolution networks for lidar-based perception,” *IEEE Transactions on Pattern Analysis and Machine Intelligence*, 2021.

[16] L. Fan, X. Xiong, F. Wang, N. Wang, and Z. Zhang, “Rangedet: In defense of range view for lidar-based 3d object detection,” in *Proceedings of the IEEE/CVF International Conference on Computer Vision (ICCV)*, 2021, pp. 2918–2927.

[17] H. Caesar, V. Bankiti, A. H. Lang, S. Vora, V. E. Liou, Q. Xu, A. Krishnan, Y. Pan, G. Baldan, and O. Beijbom, “nuscenes: A multi-modal dataset for autonomous driving,” in *Proceedings of the IEEE/CVF Conference on Computer Vision and Pattern Recognition (CVPR)*, 2020, pp. 11 621–11 631.

[18] H. Thomas, C. R. Qi, J.-E. Deschaud, B. Marcotegui, F. Goulette, and L. J. Guibas, “Kpconv: Flexible and deformable convolution for point clouds,” in *Proceedings of the IEEE/CVF International Conference on Computer Vision (ICCV)*, 2019, pp. 6411–6420.

[19] D. Maturana and S. Scherer, “Voxnet: A 3d convolutional neural network for real-time object recognition,” in *Proceedings of the IEEE/RSJ International Conference on Intelligent Robots and Systems (IROS)*. IEEE, 2015, pp. 922–928.

[20] G. Riegler, A. Osman Ulusoy, and A. Geiger, “Octnet: Learning deep 3d representations at high resolutions,” in *Proceedings of the IEEE Conference on Computer Vision and Pattern Recognition (CVPR)*, 2017, pp. 3577–3586.

[21] C. Xu, B. Wu, Z. Wang, W. Zhan, P. Vajda, K. Keutzer, and M. Tomizuka, “Squeezesegv3: Spatially-adaptive convolution for efficient point-cloud segmentation,” in *Proceedings of the European Conference on Computer Vision (ECCV)*. Springer, 2020, pp. 1–19.

[22] I. Alonso, L. Riazuelo, L. Montesano, and A. C. Murillo, “3d-mininet: Learning a 2d representation from point clouds for fast and efficient 3d lidar semantic segmentation,” *IEEE Robotics and Automation Letters*, vol. 5, no. 4, pp. 5432–5439, 2020.

[23] Y. Zhang, Z. Zhou, P. David, X. Yue, Z. Xi, B. Gong, and H. Foroosh, “Polarnet: An improved grid representation for online lidar point clouds semantic segmentation,” in *Proceedings of the IEEE/CVF Conference on Computer Vision and Pattern Recognition (CVPR)*, 2020, pp. 9601–9610.

[24] V. E. Liou, T. N. T. Nguyen, S. Widjaja, D. Sharma, and Z. J. Chong, “Amvnet: Assertion-based multi-view fusion network for lidar semantic segmentation,” *arXiv preprint arXiv:2012.04934*, 2020.

[25] M. Gerdzhev, R. Razani, E. Taghavi, and L. Bingbing, “Tornado-net: multiview total variation semantic segmentation with diamond inception module,” in *Proceedings of the IEEE International Conference on Robotics and Automation (ICRA)*. IEEE, 2021, pp. 9543–9549.

[26] F. Duerr, M. Pfaller, H. Weigel, and J. Beyerer, “Lidar-based recurrent 3d semantic segmentation with temporal memory alignment,” in *Proceedings of the International Conference on 3D Vision (3DV)*. IEEE, 2020, pp. 781–790.

[27] Z. Zhang and M. Sabuncu, “Generalized cross entropy loss for training deep neural networks with noisy labels,” *Proceedings of the Advances in Neural Information Processing Systems (NIPS)*, vol. 31, 2018.

[28] M. Berman, A. R. Triki, and M. B. Blaschko, “The lovász-softmax loss: A tractable surrogate for the optimization of the intersection-over-union measure in neural networks,” in *Proceedings of the IEEE Conference on Computer Vision and Pattern Recognition (CVPR)*, 2018, pp. 4413–4421.

[29] A. Bokhovkin and E. Burnaev, “Boundary loss for remote sensing imagery semantic segmentation,” in *Proceedings of the International Symposium on Neural Networks (ISNN)*. Springer, 2019, pp. 388–401.

[30] L. Wang, Y. Xiong, Z. Wang, Y. Qiao, D. Lin, X. Tang, and L. Van Gool, “Temporal segment networks for action recognition in videos,” *IEEE transactions on pattern analysis and machine intelligence*, vol. 41, no. 11, pp. 2740–2755, 2018.

[31] X. Chen, S. Li, B. Mersch, L. Wiesmann, J. Gall, J. Behley, and C. Stachniss, “Moving object segmentation in 3d lidar data: A learning-based approach exploiting sequential data,” *IEEE Robotics and Automation Letters*, vol. 6, no. 4, pp. 6529–6536, 2021.

[32] O. Ronneberger, P. Fischer, and T. Brox, “U-net: Convolutional networks for biomedical image segmentation,” in *Proceedings of the International Conference on Medical Image Computing and Computer-Assisted Intervention (MICCAI)*. Springer, 2015, pp. 234–241.

[33] K. He, X. Zhang, S. Ren, and J. Sun, “Deep residual learning for image recognition,” in *Proceedings of the IEEE Conference on Computer Vision and Pattern Recognition (CVPR)*, 2016, pp. 770–778.

[34] A. Geiger, P. Lenz, and R. Urtasun, “Are we ready for autonomous driving? the kitti vision benchmark suite,” in *Proceedings of the IEEE Conference on Computer Vision and Pattern Recognition (CVPR)*. IEEE, 2012, pp. 3354–3361.

[35] M. Tatarchenko, J. Park, V. Koltun, and Q.-Y. Zhou, “Tangent convolutions for dense prediction in 3d,” in *Proceedings of the IEEE Conference on Computer Vision and Pattern Recognition (CVPR)*, 2018, pp. 3887–3896.

[36] H. Su, V. Jampani, D. Sun, S. Maji, E. Kalogerakis, M.-H. Yang, and J. Kautz, “Splatnet: Sparse lattice networks for point cloud processing,” in *Proceedings of the IEEE Conference on Computer Vision and Pattern Recognition (CVPR)*, 2018, pp. 2530–2539.

[37] R. A. Rosu, P. Schütt, J. Quenzel, and S. Behnke, “Latticenet: Fast point cloud segmentation using permutohedral lattices,” *arXiv preprint arXiv:1912.05905*, 2019.

[38] S. Qiu, S. Anwar, and N. Barnes, “Semantic segmentation for real point cloud scenes via bilateral augmentation and adaptive fusion,” in *Proceedings of the IEEE/CVF Conference on Computer Vision and Pattern Recognition (CVPR)*, 2021, pp. 1757–1767.

[39] S. Li, X. Chen, Y. Liu, D. Dai, C. Stachniss, and J. Gall, “Multi-scale interaction for real-time lidar data segmentation on an embedded platform,” *IEEE Robotics and Automation Letters*, vol. 7, no. 2, pp. 738–745, 2021.

[40] Y. Zhao, L. Bai, and X. Huang, “Fidnet: Lidar point cloud semantic segmentation with fully interpolation decoding,” in *Proceedings of the IEEE/RSJ International Conference on Intelligent Robots and Systems (IROS)*. IEEE, 2021, pp. 4453–4458.

[41] R. Razani, R. Cheng, E. Taghavi, and L. Bingbing, “Lite-hdseg: Lidar semantic segmentation using lite harmonic dense convolutions,” in *Proceedings of the IEEE International Conference on Robotics and Automation (ICRA)*. IEEE, 2021, pp. 9550–9556.